4-2013

Enhancement of electron-positron pair creation due to transient excitation of field-induced bound states

M Jiang
Chinese Academy of Sciences

Q Z. Lv
China University of Mining and Technology

Z M. Sheng
Shanghai Jiao Tong University

Rainer Grobe
Illinois State University

Qichang Su
Illinois State University

Enhancement of electron-positron pair creation due to transient excitation of field-induced bound states

M. Jiang,[1] Q. Z. Lv,[2] Z. M. Sheng,[3] R. Grobe,[4] and Q. Su[4]

[1]*Beijing National Laboratory for Condensed Matter Physics, Institute of Physics, Chinese Academy of Sciences, Beijing 100190, China*

[2]*State Key Laboratory for GeoMechanics and Deep Underground Engineering, China University of Mining and Technology, Beijing 100083, China*

[3]*Key Laboratory for Laser Plasmas and Department of Physics, Shanghai Jiao Tong University, Shanghai 200240, China*

[4]*Intense Laser Physics Theory Unit and Department of Physics, Illinois State University, Normal, Illinois 61790-4560, USA*

(Received 13 September 2012; published 3 April 2013)

We study the creation of electron-positron pairs induced by two spatially separated electric fields that vary periodically in time. The results are based on large-scale computer simulations of the time-dependent Dirac equation in reduced spatial dimensions. When the separation of the fields is very large, the pair creation is caused by multiphoton transitions and mainly determined by the frequency of the fields. However, for small spatial separations a coherence effect can be observed that can enhance or reduce the particle yield compared to the case of two infinitely separated fields. If the travel time for a created electron or positron between both field locations becomes comparable to the period of the oscillating fields, we observe peaks in the energy spectrum which can be explained in terms of field-induced transient bound states.

DOI: 10.1103/PhysRevA.87.042503 PACS number(s): 31.30.J−, 12.20.Ds, 34.50.Rk, 03.65.−w

I. INTRODUCTION

In 1951 Schwinger published his analysis of the electron-positron pair-creation process in the vacuum triggered by an ultrastrong static and spatially uniform electric field [1]. This important work about the breakdown of the vacuum has received wide attention in the physics community [2]. Although the typical electric field strengths to produce a substantial amount of pairs are still hard to generate experimentally, laser technology has advanced at a rapid pace in recent years [3] to make laser based pair creation [4] an area of current interest. In addition to the motivation from the experimental side, theoretical studies of the pair-creation process by supercritical fields have attracted attention in the optics community and the research has led to many interesting results, allowing us to understand more details of this fascinating process and better preparing us for the design of future experiments that can probe relativistic quantum electrodynamics.

Theoretical studies have proposed several ways to produce or control the pair-creation process. Among these studies one approach is to use a supercritical static field (or a field that varies slowly in time), thus allowing particles to tunnel across the positive and negative energy gap reduced by the static field and creating a continuous flux of particle pairs [5–7]. This mechanism is referred to as the Schwinger tunneling effect. However, even if the fields are only subcritical there are also other mechanisms that can lead to the creation of particles. For example, time-dependent fields [8–18] can produce particles by triggering a transition between the negative and positive states through photon absorption if the frequency of the alternating field exceeds the mass gap. Many proposals have been reported to lower the pair-creation threshold by exploiting more than just one external field [19,20]. Recently, it was also proposed to use spatially localized magnetic fields to control the pair-creation process [21,22].

In a recent work, we studied how the pair-creation process could be controlled by a combination of a time-dependent force field with a static field [17]. The time-dependent field was represented by the Sauter potential [23]. The static field was intended to drag the created particles out of the interaction zone but it also caused the particles to return to the interaction zone, thus leading to a complicated dynamics. In this work, we will examine two spatially localized and time-dependent force fields with variable spatial separation. We show that quantum coherence can play a significant role during the pair creation. The two oscillatory electric fields point in opposite directions at each time. For such a configuration, new effects are predicted that cannot occur for a single oscillating field. We discuss a coherence effect between the pairs created at each localized field, which is associated with the fact that energy levels can be shifted up and down leading to the occurrence of additional transient bound states.

The paper is organized as follows. In Sec. II, we introduce the field theoretical framework for our approach and present the necessary equations for calculating the total number of created particles as well as the spatial distributions. In Sec. III we study the pair creation yields and compare the perturbative predictions with the exact data in the single-photon regime. In Sec. IV, we examine the spatial densities, energy and momentum spectra, and the role of transiently bound states in the multiphoton domain. In Sec. V, we summarize and discuss our findings.

II. THE QUANTUM FIELD THEORETICAL SIMULATIONS AND THE PERTURBATIVE APPROACH

We briefly summarize first the main idea for our numerical approach based on quantum field theory (QFT) in external fields. The time-dependent operator $\hat{\Psi}(z,t)$ for the electron-positron field can be obtained from the time-dependent Heisenberg equation as well as the Dirac equation (here and below we use atomic units) [4]. As long as we can neglect interfermionic forces, this equation is sufficient to predict the multiparticle dynamics of pair creation.

$$i\partial\hat{\Psi}(z,t)/\partial t = [c\alpha_z\hat{p}_z + \beta c^2 + V(z,t)]\hat{\Psi}(z,t). \quad (2.1)$$

For simplicity we assume that the time-dependent potential $V(z,t)$ is extended only along the z axis. Here α_z and β are the Dirac matrices and c is the speed of light ($c = 137.036$ a.u). In the appendix of Ref. [21] it was shown explicitly and illustrated numerically that the specific gauge used to represent a spatially localized electric field does not affect the pair-creation rate. We can expand $\hat{\Psi}(z,t)$ in terms of the electron annihilation and position creation operators ($\hat{b}$ and $\hat{d}^\dagger$, respectively) and the position representation of the force-free positive and negative energy eigenstates $|p\rangle$ and $|n\rangle$,

$$\hat{\Psi}(z,t) = \sum_p \hat{b}_p(t)u_p(z) + \sum_n \hat{d}_n^\dagger(t)v_n(z) = \sum_p \hat{b}_p u_p(z,t) + \sum_n \hat{d}_n^\dagger v_n(z,t). \quad (2.2)$$

Here $\hat{b}_p$ and $\hat{d}_n^\dagger$ denote the annihilation and creation operators for the electron and the positron. Note that $u_p(z,t)$ and $v_n(z,t)$ satisfy the single-particle time-dependent Dirac equation. The numerical split operator technique [24–27] can be used to obtain solutions without any approximation, and the final states of the system according to Eq. (2.2) can be obtained at any space-time point.

With the knowledge of the QFT field operator, the expectation value of the electron density operator in the vacuum can be expressed according to

$$\rho(z,t) \equiv \langle\langle \text{vac}\|\hat{\Psi}_e^\dagger(z,t)\Psi_e(z,t)\|\text{vac}\rangle\rangle, \quad (2.3)$$

which is the electronic number density. Here $\hat{\Psi}_e = \Sigma_p \hat{b}_p(t)\, u_p(z)$ denotes the electronic portion of the field operator. This particular definition leads to a certain interpretation of the observables computed inside the interaction zone. All probabilities shown correspond to the amount of electron-positron pairs after the electric field has been turned off abruptly. The values therefore include also the unavoidable pair creation or annihilation associated with the temporal turn off. For a more detailed discussion, see [18,28]. After some operator algebra, the result can be expressed via the field-free positive and negative energy eigenstates $|p\rangle$ and $|n\rangle$ of the single-particle Dirac Hamiltonian and the associated single-particle evolution operator $U(t)$ as

$$\rho(z,t) = \sum_n \left| \sum_p U_{p,n}(t)u_p(z) \right|^2, \quad (2.4)$$

where $U_{p,n} \equiv \langle p|U(t)|n\rangle = \langle p|n(t)\rangle$. Here the initial states $|n(t=0)\rangle$ are the energy eigenstates associated with the negative energy continuum. By integrating Eq. (2.4) over space, we can get the total number of created pairs as

$$N(t) \equiv \int dz\, \rho(z,t) = \sum_{p,n} |U_{p,n}(t)|^2. \quad (2.5)$$

These expressions permit us to study the details of the pair-creation process for various parameters such as potential height, width, and frequency of the oscillating fields by investigating the total number of created pairs as well as their spatial and momentum distributions. For an alternative approach based on in and out states, see, e.g., [29]. While this approach leads to the same result [30,31] as the asymptotic in- and out-state-based S-matrix formalism after the external field is turned off, it permits us to follow the dynamics with space-time resolution.

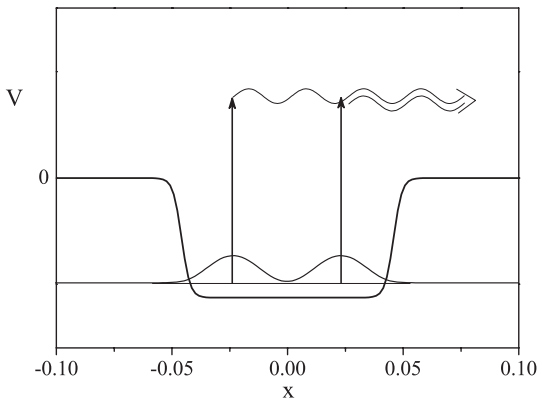

FIG. 1. Sketch of the space and time-dependent potential used in our calculations. The created waves due to photon absorption and their initial spacing characteristic of the two-peaked bound state may cause resonances in the pair-creation yield.

To model two spatially localized fields, we define $V(z,t) \equiv V_0 \sin(\omega t)[S(z - D/2) - S(z + D/2)]$ shown in Fig. 1. Here $S(z)$ represents the Sauter potential [23] function $S(z) \equiv 1/2\,[1 + \tanh(z/W)]$ with the width W of each field, and D denoting the separation between the two localized electric fields. For such a configuration that varies in time with frequency ω, particles can be created via the absorption of an integer number of photons. The potential configuration corresponds to two dislocated oscillatory electric fields that have identical intensities, but frequencies differ by an overall phase shift of π. For such a model potential, new effects are predicted that cannot occur for a single oscillating field. It creates particles with coherent frequency and certain phase difference and enables us to study quantum interference effects. We show that quantum coherence can play a significant role during the pair creation. For such potential well configuration, transient bound states should appear, and we intend to study their effect on the pair-creation process. The energy levels shift up and down in time leading to the occurrence of additional transient bound states.

The states in the negative energy manifold can absorb one or a multiple number of photons with energy ω each. The absorption of photons connects the negative and the positive energy states to effectively bridge the energy gap in between and thus creates the pairs.

Our numerical simulations naturally include photon transitions of all orders. But to obtain a first understanding of the process we examine the lowest number of relevant photon absorption schemes. For instance, for the single-photon absorption, the energy threshold for pair creation corresponds to the condition $\omega > 2c^2$. Such a process has been confirmed to be a viable picture for interpreting numerical results [17]. When the photon frequency is gradually increased, the pair creation is observed to start after ω exceeds $2c^2$, which is equal to the gap between the negative and positive energy levels. It is worth mentioning that the usual condition of supercriticality requires the potential height V_0 to exceed the energy gap $2c^2$. Since both fields are time dependent, the critical condition for the pair creation is mainly determined

by the frequency ω, while the total yield is proportional to ${V_0}^2$. As a result the potential strength can be much less than $2c^2$ and technically subcritical, while still triggering the photon-induced pair creation.

To describe the few-photon absorption theoretically, we consider first time-dependent perturbation theory. As the interaction does not couple different spin directions, we can express the field operator by only two components. The Hamiltonian of this system can then be separated in two parts: $H = H_0 + H'$, where $H_0 = c\sigma_1 p + \sigma_3 c^2$ is the force-free Hamiltonian, and the external field is represented by the interaction Hamiltonian $H' = V_0 \sin(\omega t)\,[S(z - D/2) - S(z + D/2)]$ treated as a perturbation. Here σ_1 and σ_3 are the Pauli matrices. The eigenvalues and eigenvectors of H_0 can be found analytically, as E_p and $u_p(z)$ for the positive energy, and E_n and $v_p(z)$ for the negative energy. The first-order transition amplitude from the negative state $|n\rangle$ to the positive state $|p\rangle$ at an arbitrary time t is given by

$$C_{pn}^{(1)} = \frac{1}{i}\int_0^t \langle p|H'|n\rangle e^{i(E_p - E_n)\tau}\, d\tau. \tag{2.6}$$

After some algebra, we obtain the following expression:

$$C_{pn}^{(1)} = \frac{\pi W V_0}{L}\frac{\sin[(\omega_{pn} - \omega)t/2]}{[(\omega_{pn} - \omega)/2]} A_{pn} \operatorname{csch}\left[\frac{\pi W (p+n)}{2}\right] \times \sin[(p+n)\,D/2]\,. \tag{2.7}$$

Here the term associated with the inner product A_{pn} is defined as

$$A_{pn} = \frac{\operatorname{sgn}(n)\sqrt{E_p + c^2}\sqrt{-E_n - c^2} + \operatorname{sgn}(p)\sqrt{E_p - c^2}\sqrt{-E_n + c^2}}{4\pi\sqrt{-E_p E_n}}. \tag{2.8}$$

By summing over all the states of p and n, we can obtain the first-order perturbation estimation of the total pair production as

$$N^{(1)}(t) = \sum_{pn} |C_{pn}^{(1)}|^2. \tag{2.9}$$

With the help of Eq. (2.7) the first-order perturbative result can be obtained as

$$N^{(1)}(t) = \frac{\pi^4 W^2 V_0^2}{2L^2}\sum_{p,n}\frac{\sin^2[(\omega_{pn} - \omega)t/2]}{[(\omega_{pn} - \omega)/2]^2} A_{pn}^2 \operatorname{csc} h^2\left[\frac{\pi W (p+n)}{2}\right] 2\sin^2[(p+n)\,D/2]\,. \tag{2.10}$$

Except for the last sinusoidal term $2\sin^2[(p+n)D/2]$, such an expression describes exactly twice the yield associated with a single localized field. The potential well width D enters the expression only via this additional factor, thus resulting in an oscillatory behavior. Notice that this term is independent of time, therefore such an oscillation also manifests itself in the creation rate, which is defined as the slope of $N^{(1)}(t)$. The fact that the spacing D between both fields can modify the rate associated with two infinitely apart fields by a factor between 0 and 2, suggests that we can have a reduction as well as an enhancement of the pair-creation process. The possibility of an enhancement is rather unexpected as the binding of fermions usually lowers the pair-creation rate due to Pauli blocking [6]. In the limit of large D the extra factor $2\sin^2[(p+n)D/2]$ approaches 1 so Eq. (2.10) predicts the total number of pairs for two single fields, as is expected.

III. COHERENCE EFFECTS IN THE SINGLE-PHOTON REGIME ($\omega > 2c^2$)

To examine the validity of the first-order perturbative prediction from the previous section, we first choose a frequency $\omega = 2.5c^2$. Such a frequency enables the single-photon absorption to bridge the negative and the positive energy states, even though the value of $V_0 = 1.5c^2$ is chosen to be subcritical from an energetic point of view. One could refer to subcritical potentials that can continuously produce pairs due to single or multiphoton transitions as *temporally supercritical*. In Fig. 2(a) we present the time evolution of the total number of pairs created, for five different potential well widths $D = 2/c$, $4/c$, $6/c$, $8/c$, and ∞. For an infinite width, we recover the yield generated by two single localized fields. For comparison, the dashed line in Fig. 2(a) denotes twice the production associated with a single localized field. Due to the condition $\omega = 2.5c^2 > 2c^2$, pairs are created continuously at a constant rate. Obviously, for different well separations, the creation rates yield different values. Such a change in the creation rate with different D is a coherence effect, which is due to the interference of the created particles from both localized fields. Note that although there exists an oscillatory behavior brought about by D, in this particular case, the pair creation produced by two infinitely extended fields (dashed line) take the largest value. Note also the change in pair creation in Fig. 2(a) is not monotonic with the increase of D. Such a nonmonotonic feature can be associated with Pauli blocking and will be discussed further below. For the parameters in Fig. 2(a), the numerical results deviate from the perturbative result due to a too large V_0. Below we will show that for a smaller V_0 the perturbative results are highly accurate.

In order to show that the nonmonotonic dependence of the total pair production as a function of D is not sensitive to the type of turn off, we have repeated the same simulation with identical parameters as in Fig. 2(a), except that the external field was turned off smoothly (and not abruptly). As expected, the data in the inset of Fig. 2(a) suggest that the dependence on D occurs during the interaction, independent of details of how the field was turned off.

Equivalently, perturbation theory also becomes more valid if the width W of the corresponding potential well is increased, leading to smaller electric fields. We show in Fig. 2(b) that the

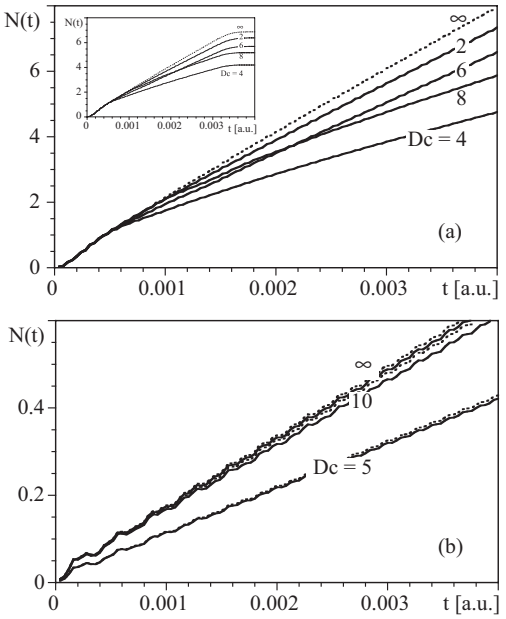

FIG. 2. (a) Graph of the total pair production as a function of time (in a.u.), for the potential well widths $D = 2/c$, $4/c$, $6/c$, $8/c$, and ∞ (dashed line). The inset shows the data for the case where the external field has been smoothly turned off. Other parameters used in our simulations are $V_0 = 1.5c^2$, $W = 0.5/c$, and $\omega = 2.5c^2$. (b) Same as in (a) but with $W = 3/c$, $\omega = 3c^2$ and $D = 5/c$, $10/c$, and ∞. The corresponding perturbative results are in dashed lines.

discrepancy is indeed smaller for $W = 3/c$ and $\omega = 2.5c^2$. But in this case the variation with different D is monotonic and not oscillatory as in Fig. 2(a).

We next investigate the pair creation as a function of the field frequency ω. As shown in Fig. 3, the pair production is significantly enhanced at the threshold $\omega = 2c^2$. This frequency couples the edges of the upper and lower energy levels by a single photon. A second, but much weaker enhancement that develops into a plateau is also visible in the figure. It starts at the smaller frequency $\omega = c^2$ and can be attributed to a two-photon transition. Our numerical accuracy does not allow us to determine the three-photon enhancement threshold starting at $\omega = 2c^2/3$ (not displayed). For finite spacings D,

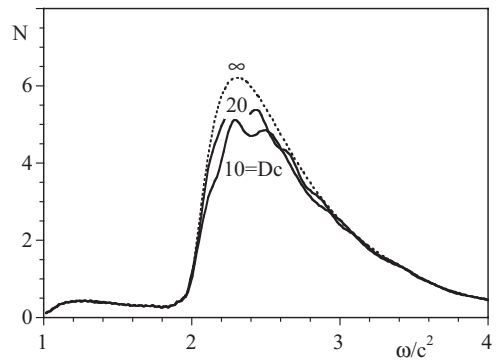

FIG. 3. The total pair production as a function of frequency of the oscillating fields at $t = 0.004$ for three potential well widths $D = 10/c$, $20/c$, and ∞ (dashed line). Other parameters used in our simulations are $V_0 = 1.5c^2$, $W = 1/c$.

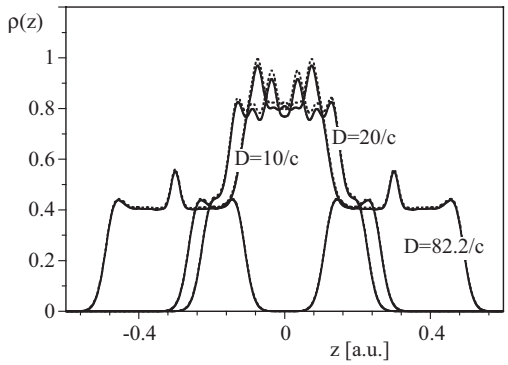

FIG. 4. The spatial probability density of the created electrons for three different potential well spacings D (as indicated) for $\omega = 3c^2$. Other parameters used in the simulations are $t = 0.002$, $V_0 = 1.5c^2$, and $W = 3/c$. The bold lines are simulation results and the dashed lines are the perturbative results.

the general shape of distribution which is peaked at around $\omega = 2.4c^2$ is nearly identical for small and large frequencies ω. In addition to this peak at $2.4c^2$ we also observe an oscillatory dependence of ω for finite values of D, which, however, for $D \to \infty$ disappears.

To roughly estimate the possible modulation frequency for the case of $D = 10/c$ one could consider the formation of a standing classical wave between the edges of a potential well with separation D. The longest permitted wavelength $\lambda \sim 2D$ corresponds to a wave number $k = 2\pi/\lambda = 2\pi/(2D) = \pi/D$. If we furthermore assume c as the speed then the associated frequency would be $\omega = ck = c\pi/D$. For $D = 10/c$ this amounts to $\omega = 0.314c^2$, which differs from the modulation frequency $0.23c^2$ that can be read off of Fig. 3. However, for $D = 20/c$ the same estimate leads to $\omega \sim 0.157\, c^2$; comparing to the value found in Fig. 3 ($0.15c^2$), the match is better than 4.7%.

Next we investigate the spatial distributions associated with the yields displayed in Fig. 2. We can see in Fig. 4 that the electrons created from the two fields leave the interaction region as they are accelerated outwards by the two edges of the potential well that produced them. The locations of the fields agree with the maxima of the electronic densities. For comparison, the dashed lines are the perturbative results. For small D, the mismatch amounts to around 2.89% but as D increases the agreement with the perturbation theory becomes better than 2.3%. Agreements are also found for the momentum distribution (not shown) with an agreement better than 1.57%. We should mention that the case of $D \to \infty$, of course, cannot be studied in a finite simulation. We chose here a distance $82.2/c$ (half of the numerical box length), which guarantees that the created particles can not meet on the time scales of our simulation.

To observe the effect of the potential well width on a larger scale, we calculate the pair production at a specific time $t = 0.004$ for D in the range between 0 and $20/c$. We also choose a supercritical frequency $\omega = 3c^2$, which yields a maximum production at energy $E = 1.5c^2$ corresponding to a single-photon transition.

In Fig. 5 we show the number of created pairs at final time 0.004 as a function of the spacing D for $W = 0.5/c$, $1/c$,

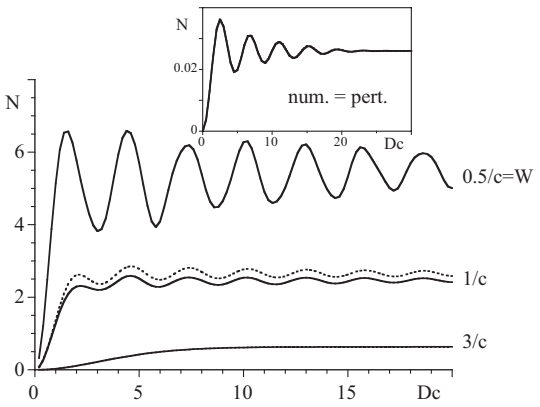

FIG. 5. The created pairs as a function of the potential well separation D, for field widths of $W = 0.5/c$, $1/c$, and $3/c$, at a specific time $t = 0.004$. The dashed line shows the perturbative result for $W = 1/c$ ($V_0 = 1.5c^2$, $\omega = 3c^2$). The inset shows the perfect agreement between the exact and the perturbative yield for a smaller potential $V_0 = 0.1c^2$ ($W = 0.5/c$, $\omega = 2.5c^2$, $t = 0.002$).

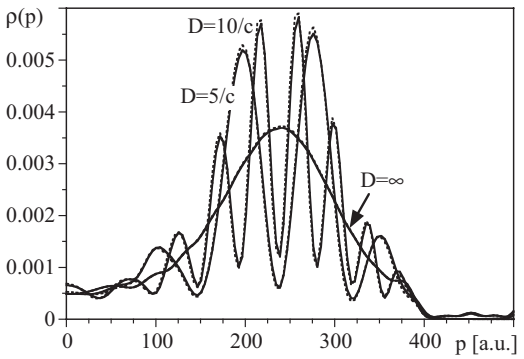

FIG. 6. Momentum spectrum of the created pairs at $t = 0.002$, with parameter $V_0 = 1.5c^2$, $W = 1/c$, and $\omega = 4c^2$, for $D = 5/c$, $D = 10/c$, and $D = \infty$. The dashed lines represent the corresponding perturbative results.

and $3/c$. This interaction time was chosen large enough, such that even for the largest value of D ($=20/c$) the particles had sufficient time to travel back and forth between both electric fields. As D increases further, all curves evolve to a (D-independent) constant as the corresponding time 0.004 is too short to allow the particles created at $z = -D/2$ to interfere with the process at the other field at $z = D/2$.

As for a given potential height V_0 the corresponding electric field amplitude increases with decreasing width W, a smaller W results in an overall larger amount of pair creation reflected by an increased mean level of the oscillatory curves. Note that for $W = 0.5/c$ the dynamics cannot be described by simple perturbation theory. For example, the mean level for $D < 10/c$ is $N = 5.15$, and for $D \geqslant 10/c$ the average moves to $N = 5.43$. For $D \to \infty$, the production approaches 5.83.

Note the oscillations are present for $D = 3/c$ as well, but they are very small in magnitude and therefore invisible in the graph. According to the perturbative theory in Sec. II, as $D \to \infty$, the last term in Eq. (2.10), or $2\sin^2[(p+n)D/2]$, approaches 1, corresponding to two times the single field result, which is expected. Eqution (2.10) also suggests that while $D \to \infty$ the term $(p + n)$ tends to be zero as the limit of the quadratic sine term leads to $\delta(p+n)$. For such a limit, the csch term approaches $1/(p+n)^2$, thus reducing the amplitude of oscillation caused by D.

We have noted in the prior section the important result that the total yield predicted by perturbation theory can either enhance or decrease depending on D. In the inset we display the yield for the smaller potential $V_0 = 0.1c^2$, where we have a perfect agreement between the exact and the perturbative yield. Here it is obvious that we obtain the largest yield ($N \approx 0.036$) for about $D = 2.5/c$, while the yield for $D \to \infty$ with $N \approx 0.025$ is less. Due to the double integral over the momentum in Eq. (2.10), it is very difficult to realize the maximum possible amount of enhancement (a factor of 2) relative to the yield for $D \to \infty$.

It is interesting to note that the period of oscillation for $W = 0.5/c$ and $1/c$ are rather similar and around $\sim 2.8/c$. According to the sinusoidal term in Eq. (2.10), the period should be related to $\sin^2[(p+n)D/2]$. By considering the maximum pair production at $E = 1.5c^2$, or from the negative state with momentum $n = \pm 153.2$ to the positive state with momentum $p = \pm 153.2$, we expect the period of oscillation to be around $2.81/c$, which matches quite well with our observation in the simulation results, with an agreement of around 1%.

In Fig. 5, for the field width $W = 1/c$, we have also presented the perturbation results according to Eq. (2.10) with the dashed curve. However, the validity of such perturbative approximation is limited to low intensities and short times. Since we assign an electric field with amplitude $V_0/(2W) = 0.75c^3$, and a relatively long time $t = 0.004$, the error turns out to be around 9%, but the qualitative behavior is basically reproduced.

According to the term $\sin^2[(p+n)D/2]$ in Eq. (2.10), one could also expect oscillations in the momentum distribution, with a period $T_p = 86.06$ and 43.03 for $D = 5/c$ and $10/c$, respectively. To test this hypothesis, we graph in Fig. 6, the corresponding number densities in the momentum space for the same parameters. For an infinite D we find a wide and singly peaked distribution with a maximum located at $k = 237.3$ corresponding to an energy of $E = \omega/2$. This energy is expected as it corresponds to a momentum-conserving single-photon transition (here $\omega = 4c^2$) from the lower to the upper energy continuum. In the special case for which the external force is spatially independent ($W \to \infty$), only momentum-conserving transitions would be permitted favoring transitions that are nearly symmetric about $E = 0$, between the positive and the negative energy manifolds [32]. Although each field's width W is not so wide, the conservation in momentum still influences the location of the peak in energy here.

As we decrease the spacing D, we observe the predicted oscillatory behavior. The observed periods (in k) from the simulation are 87.1 (for $D = 5/c$) and 43.6 (for $D = 10/c$) and deviate less than 2% from the perturbative results.

Let us also present the spatial distribution for $\omega < 2c^2$. The probability distributions at time $t = 0.0015$ are displayed in Fig. 7. The wavelengths of the spatial oscillations outside of the interaction area have similar maxima and minima for different potential well separations D. The periodicity of the maxima according to the data is $\lambda = 0.043$ and 0.029 for

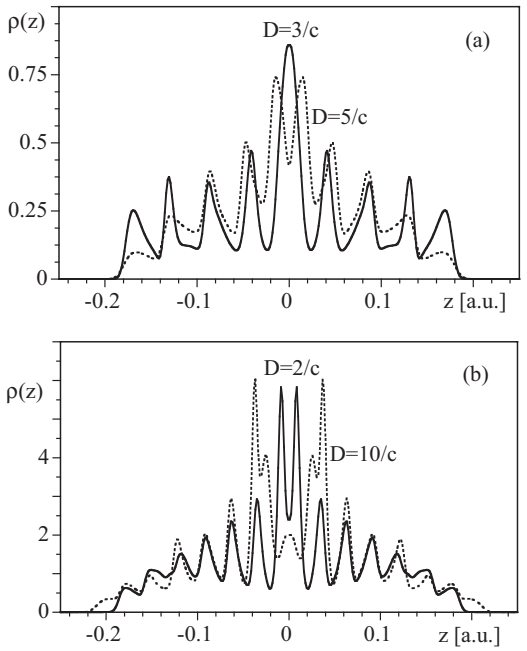

FIG. 7. The probability density of the created electrons of two different potential well widths D, for (a) $\omega = c^2$ and (b) $\omega = 1.5c^2$. Other parameters used in the simulations are $t = 0.0015$, $V_0 = 1.5c^2$, and $W = 0.5/c$.

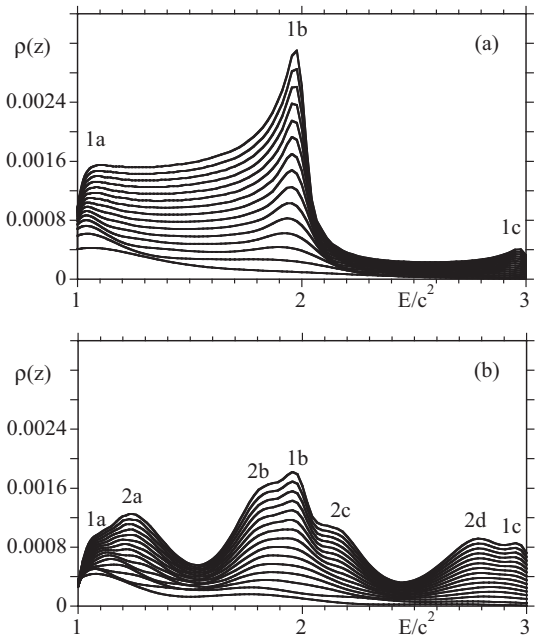

FIG. 8. The time evolution of the energy spectrum from $t = 0$ to 5×10^{-3}, with interval $\Delta t = 3.34 \times 10^{-4}$, and $V_0 = 1.5c^2$, $W = 0.5/c$, and $\omega = c^2$, for potential well separations (a) $D \to \infty$ and (b) $D = 3/c$.

$\omega = c^2$ and $1.5c^2$, respectively. These spatial oscillations may be related to the temporal variation of the field, rather than to the coherent interferences due to both fields. This suggests that we obtain a maximum of bursts when the electric fields are maximum. In fact, the numerical values of the corresponding wavelengths $\lambda = 2\pi c/\omega$ leads to $\lambda = 0.044/c$ (for $\omega = c^2$) and $\lambda = 0.029/c$ ($\omega = 1.5c^2$). The agreement with the predictions is rather good as the deviation is less than 2.3%.

It is interesting to see that while the D dependence showed up in the frequency graph of Fig. 3, the dependence on ω is apparent in the spatial distributions in Fig. 7. Note that also the location of the peaks does not depend on D.

IV. ENERGY SPECTRA AND TRANSIENT BOUND STATES IN THE MULTIPHOTON REGIME ($\omega = c^2$)

In this section we will analyze the energy spectra of the created electrons. We will see that the spacing D of the two electric fields has a significant impact on the energy distributions. For a steady potential well that does not vary with time, some bound states are formed, with discrete energy levels. In this case, some uppermost negative levels could shift up from $-c^2$, and thus would be closer to the positive levels. Below we will show that such a phenomenon can also occur for a time-dependent potential for a certain relationship of the temporal characteristics of the dynamics. The first one is the time it takes to form these discrete energy levels, which we denote by T_1. Here in our model, it may be considered as the time that created particles at one edge need to travel to the other edge, which is approximately D/c. The second time scale is obviously given by the period of the potential $T_2 = 2\pi/\omega$. As long as T_1 and T_2 are comparable, we might expect that the shifts of energy levels are relevant for the electron spectra.

To set the scale, let us first examine in Fig. 8(a) the energy spectra for the case of two independent fields that are infinitely apart ($D \to \infty$). The simulation extends from $t = 0$ to 0.005 (15 cycles) with an interval $\Delta t = 3.34 \times 10^{-4}$. We only focus on the location of energy peaks here.

At very early times (lower graphs) the spectra are rather monotonic and peaked at lower energies. They are associated with the details of the turn on. As we increase the interaction time we observe the occurrence of three peaks with energies corresponding to the absorption of two, three, and four photons from the negative energy edge of $-c^2$. For comparison with the data for an infinite D, we label the three peaks 1a, 1b, and 1c. For the spectra in Fig. 8(b) we have repeated the same simulation, but this time we chose a finite spacing of $D = 3/c$. The small frequency ω and potential well separation D make the two characteristic times T_1 and T_2 comparable. We now observe that in addition to three peaks, a set of four additional peaks has been created in addition to the rather pronounced minima close to $E = 1.5c^2$ and $E = 2.5c^2$. The energies of the new peaks are 1.24 (labeled as 2a), 1.80 (2b), 2.15 (2c), and 2.78 (2d).

As we will discuss in detail below, these additional peaks are a direct manifestation of the transient formation of bound states, which can shift in and out of resonance and therefore enhance the pair creation for electron-positron pairs with a specific set of energies. To confirm this assessment, we have calculated the instantaneous energy spectra of the system within one temporal period.

In Fig. 9 we display the instantaneous energy eigenvalues of the continuous as well as the discrete states as a function of time within one temporal period, by diagonalizing the Dirac Hamiltonian at every instant of time. During the first half of the laser period the potential is attractive for a positron, which

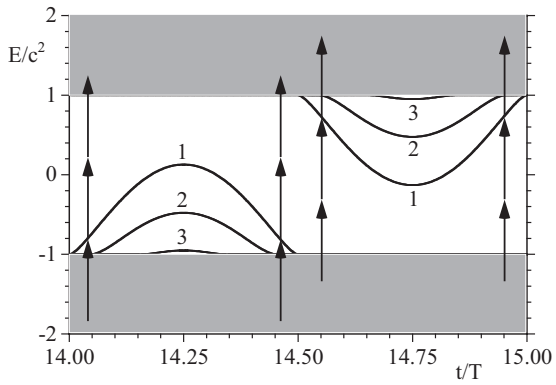

FIG. 9. Instantaneous eigenvalues of the potential well in one temporal period with width $D = 3/c$, while $V_0 = 1.5c^2$ and $W = 0.5/c$, the same parameters as for Fig. 7.

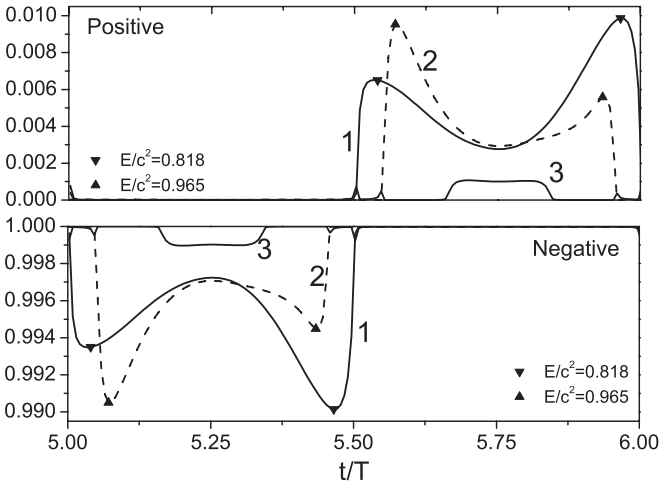

FIG. 10. The excitations of the three bound states during one temporal period with width $D = 3/c$ ($V_0 = 1.5c^2$, $W = 0.5/c$, the same parameters as for Fig. 8).

leads to the emergence of three bound states from the lower energy continuum. During the second half each of the two fields point in the opposite direction, producing a potential that is attractive for the electron, leading to the transient occurrence of three bound states that have emerged from the positive energy continua. The three maximum bound state energies are at $\pm 0.13c^2$ (state 1), $\pm 0.47c^2$ (state 2), and $\pm 0.94c^2$ (state 3). While the third bound state remains very close to the corresponding edges of the continuum states (at energy $\pm c^2$), the maximum values of the first and second discrete states suggest rather large shifts. As the instantaneous energies of the discrete states vary significantly over each period at first, it is not clear which particular energy value is relevant with regard to the set of additional energy peaks.

In order to test directly the involvement of these transient discrete states for the creation dynamics and to possibly identify characteristic energies we have computed their total population. As indicated in Sec. II, the quantum field theoretical data were obtained by solving the Dirac equation repeatedly for any possible state in the entire Hilbert space for negative energies. During each of these simulations we monitored the excitation of the (instantaneous) three discrete states. These instantaneous bound states are denoted by $|B_t\rangle$. Note that these are not solutions to the time-dependent Dirac equation. The excitations shown in Fig. 10 are calculated as $\Sigma_n |\langle B_t | n(t)\rangle|^2$, which can take any value between 0 and 1.

In Fig. 10 we present the time evolution of these excitations. The evolution of each period does not change too much from period to period, so we chose the time interval corresponding to the sixth cycle. The probability of the first and second bound state is apparently bigger than the third one, and they both have a two-peak distribution, which exceeds each other alternately in time. The bottom figure shows the excitations of the discrete state that are upshifted from the negative energy continuum. As in our simulation these states are initially populated as $|B_{t=0}\rangle = |n(t = 0)\rangle$ for energy $-c^2$; their population is initially equal to 1. It is interesting that it then loses precisely the same amount of population as the corresponding downshifted level from the upper continuum gains.

The triangular symbols (pointing up or down) superimposed on the excitation curves for the first and second bound states denote the value of corresponding energy of the energy level at the moment when the excitation is temporarily at its maximum value (or minimum for negative energies.). In view of the rather symmetric shape of the discrete energies as a function of time for each half-period in Fig. 9, it should be clear that the two excitation maxima correspond to the same energy value. For the first bound state this characteristic energy is $E_{1\pm} = \pm 0.818c^2$, while for the second discrete state we obtain $E_{2\pm} = \pm 0.965c^2$.

In addition to their significance with regard to their maximum degree of excitation, these characteristic energies also play a key role with regard to the observed energy peaks in the electron spectrum. It turns out that if we add two photons ($\omega = c^2$) to the energy $E_{1-} = -0.818c^2$, we approach with $1.18c^2$ the location of energy peak 2a (measured as $1.24c^2$ in Fig. 8). If we add three photons to E_{1-} we obtain $2.18c^2$, which is rather close to peak (2c) with energy $2.15c^2$.

Very similarly, if we add one photon to the characteristic energy associated with the first discrete state (from the positive energy manifold with $E_{1+} = 0.818c^2$), we obtain $1.818c^2$, which matches nearly perfectly the energy of the peak (2b) ($1.80c^2$). A two-photon transition from E_{1+} brings us to energy $2.818c^2$, once again in agreement with the energy of peak (2d), $2.78c^2$.

The characteristic energies $E_{2\pm} = \pm 0.965c^2$ of the second bound state are rather close to the edge of the continuous states, thus transitions via this discrete state would predict the energy peak locations $0.035c^2$, $1.035c^2$, $1.965c^2$, and $2.965c^2$. As apparent from Fig. 8, these specific locations would blend in with the main multiphoton peaks 1a, 1b, and 1c.

As the final ultimate test for the correspondence between the characteristic energies of the transient discrete states and the electrons' energy spectrum, we have repeated the simulation for a periodic potential that is constantly zero during each first (or second) half of each period. In this case the potential never can reverse its sign and would be always binding (or repulsive) at each time for the electron. The details of the simulations can be found in the Appendix. They perfectly confirm our above findings.

V. SUMMARY

The details of the pair-creation process under a time-dependent potential well configuration are investigated in this paper. According to our analysis, rather than the multiphoton effect that dominates the one-step time-dependent potential that we studied before, coherent and potential well effects can be observed under such field configuration. For a temporally supercritical potential with relatively wide potential well separation, the coherent effects appear and result in characteristic oscillations, which can be predicted by a first-order perturbative analysis. The potential well effect is limited to the specific condition that D/c is comparable to $2\pi/\omega$, while the time scale of the temporally varying system is slow enough to detect the bound states that are created by the potential well. As a result, new peaks emerge in the energy distribution. By varying the corresponding spacing D, the total production can be controlled in such a configuration.

Note that the corresponding peaks in the energy spectrum Fig. 8(b) and their relations with the bound state level structure in Fig. 9 are rather similar to the photoionization energy spectrum with peaks that were due to the sweeping though Rydberg levels [33].

There are, of course, many questions that can be raised. For example, the reduction of pair creation due to Pauli blocking [6] should change with D, due to particles created at one edge that arrive at the other edge. In Fig. 4 slight upshift of the oscillation center was observed, and for $\omega = 2.5c^2$ such shift is more obvious, which is absent in the perturbation result. In this model it is hard to distinguish the Pauli blocking effect from the coherence effect. It would be interesting to see what happens if one chooses the bosonic system [34,35] for which the suppression is expected to turn into an enhancement.

Also, notice that in Fig. 8 the location of the nth-order photon peaks are not exactly at $n\omega$, which could be explained as a breakdown of momentum conservation due to small field width which we used. Such a displacement from $n\omega$ may also be due to the pondermotive shift caused by the potential. Moreover, a more systematic analysis could answer why only finite bound states participate in the pair-creation process. Below the second bound state, there also exists a third bound state that is very close to the edge of the continuous state, but its influence is ignorable since it yields a deviation of only $0.01c^2$ in the time average. We note that bound states are important in the pair creation in heavy ions and also in magnetic controlled pair-creation. An analysis of those cases may help to confirm the multipeak energy structure we discovered in this work.

ACKNOWLEDGMENTS

We enjoyed several helpful discussions with Y. Liu, Dr. Y. J. Li, Dr. Y. T. Li, Dr. X. Lu, Dr. C. Müller, Dr. R. Wagner, and Dr. J. Zhang. This work has been supported by the NSF and the NSFC (Grant No. 11128409 and 11121504). Q.S. acknowledges the kind hospitality offered by the CAS during his sabbatical leave where the project was initiated.

APPENDIX

Below we examine the validity of the direct correspondence between the characteristic energies of the transient discrete states and the electrons' energy spectrum for a more general situation in which the potential is always repulsive for the electron. To achieve this we formally replace the time dependence $\sin(\omega t)$ in the potential by a new function that has been truncated to zero for $2n\pi < \omega t < (2n+1)\pi$, but remains unchanged $\sin(\omega t)$ for $(2n-1)\pi < \omega t < 2n\pi$. We denote the simulations where the *f*irst (*s*econd) *h*alf of each period has been *t*runcated by FHT (SHT). In the case of an FHT simulation, the periodic potential is always repulsive for the electron, and therefore attractive for the positron. In other words, for a FHT simulation we expect the discrete levels to arise solely from the lower energy continuum and as a result only a single set of additional peaks, corresponding to those that we labeled 2a and 2c in Fig. 8(b). The corresponding SHT

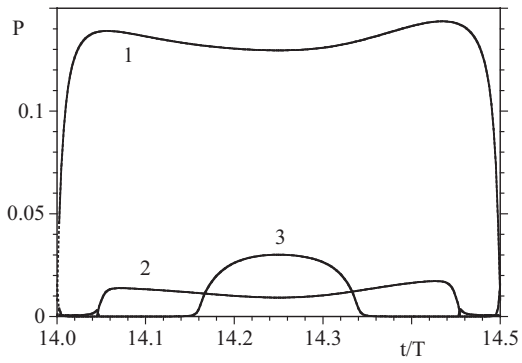

FIG. 11. The bound state excitations for a periodically truncated external potential. All other parameters as in Fig. 10.

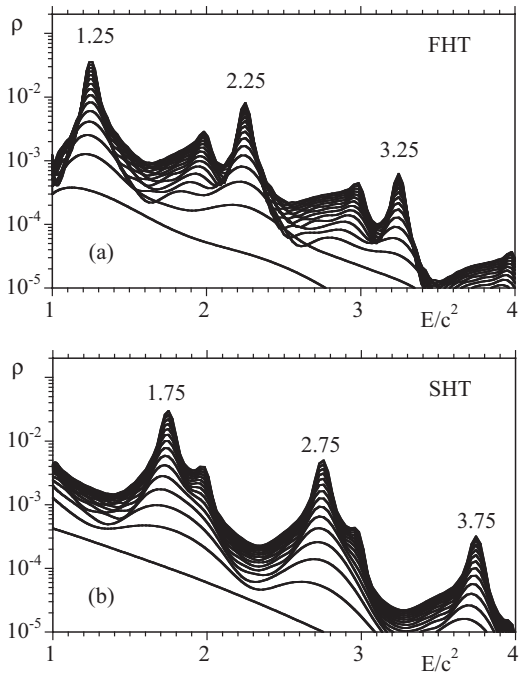

FIG. 12. The time evolution of the created electron energy spectrum for the simulation in which the potential is only on during the second half of each period (left). For the spectrum on the bottom of the potential during the second half of each cycle is truncated to zero.

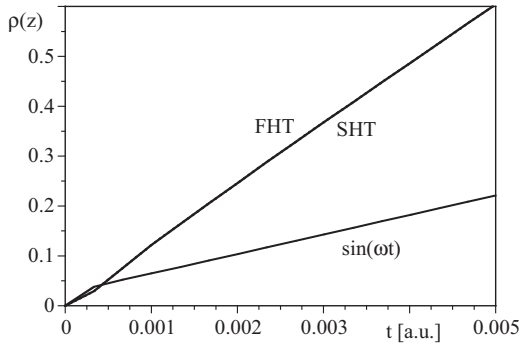

FIG. 13. The total yield after each cycle for the two temporally truncated force fields, and the normal (untruncated) force proportional to $\sin(\omega t)$. (Other parameters are as in Fig. 10.)

simulation should lead to a different set of complementary peaks. This rather "mathematical" truncated function therefore has the advantage of permitting us to analyze the contributions from each discrete state separately.

In Fig. 11 we display the corresponding excitations of the discrete states; however, the results for the upshifted simulation were shifted by half a period to the left. In order to illustrate the expected symmetry, we have also graphed one minus the excitation for the negative state instead of the excitation itself. In this situation the maximum excitation occurs at times when the corresponding energy of the bound states is around the values $E_{1\pm} = \pm 0.75c^2$ and $E_{2\pm} = \pm 0.95c^2$. In contrast to the full-cycle simulation (where we obtained the corresponding characteristic energy $E_{1\pm} = \pm 0.818c^2$), this new value for $E_{1\pm}$ is slightly less. We therefore would predict for the FHT simulation the energy peaks at locations $E_{1-} + n\omega = 1.25c^2$, $2.25c^2$, and $3.25c^2$, while for the SHT simulation the energies $E_{1+} + n\omega = 1.75c^2$, $2.75c^2$, and $3.75c^2$. The data in Fig. 12 very accurately confirm this prediction.

As a last point we should mention that the total yield associated with each (field-truncated) simulation is almost twice that of the yield of the force that is proportional to $\sin(\omega t)$. The finding displayed in Fig. 13 might be surprising at first, as in the two truncated cases the force is zero for practically half of the simulation. But in the case of the truncated force, the electrons are always ejected into the same spatial direction, whereas the periodic sign reversal for the $\sin(\omega t)$ force periodically returns the created particle to the interaction zone where they can inhibit the pair creation due to Pauli blocking.

[1] J. S. Schwinger, Phys. Rev. **82**, 664 (1951).
[2] W. Greiner, B. Müller, and J. Rafelski, *Quantum Electrodynamics of Strong Fields* (Springer Verlag, Berlin, 1985).
[3] For a proposal for the development of the ELI program, see http://www.extreme-light-infrastructure.eu
[4] H. Hu, C. Müller, and C. H. Keitel, Phys. Rev. Lett. **105**, 080401 (2010).
[5] For a review, see, e.g., S. S. Schweber, *An Introduction to Relativistic Quantum Field Theory* (Harper & Row, New York, 1962).
[6] P. Krekora, Q. Su, and R. Grobe, Phys. Rev. Lett. **92**, 040406 (2004).
[7] A. Di Piazza, E. Lötstedt, A. I. Milstein, and C. H. Keitel, Phys. Rev. Lett. **103**, 170403 (2009).
[8] E. Brezin and Itzykson, Phys. Rev. D **2**, 1191 (1970).
[9] V. S. Popov, JETP Lett. **13**, 185 (1971).
[10] V. M. Mostepanenko and V. M. Frolov, Sov. J. Nucl. Phys. **19**, 451 (1974).
[11] J. C. R. Bloch, V. A. Mizerny, A. V. Prozorkevich, C. D. Roberts, S. M. Schmidt, S. A. Smolyansky, and D. V. Vinnik, Phys. Rev. D **60**, 116011 (1999).
[12] R. Alkofer, M. B. Hecht, C. D. Roberts, S. M. Schmidt, and D. V. Vinnik, Phys. Rev. Lett. **87**, 193902 (2001).
[13] Q. Su and R. Grobe, Laser Phys. **17**, 92 (2007).
[14] R. Schützhold, H. Gies, and G. Dunne, Phys. Rev. Lett. **101**, 130404 (2008).
[15] T. Cheng, Q. Su, and R. Grobe, Phys. Rev. A **80**, 013410 (2009).
[16] G. R. Mocken, M. Ruf, C. Müller, and C. H. Keitel, Phys. Rev. A **81**, 022122 (2010).
[17] M. Jiang, W. Su, Z. Q. Lv, X. Lu, Y. J. Li, R. Grobe, and Q. Su, Phys. Rev. A **85**, 033408 (2012).
[18] C. C. Gerry, Q. Su, and R. Grobe, Phys. Rev. A **74**, 044103 (2006).
[19] S. S. Bulanov, V. D. Mur, N. B. Narozhny, J. Nees, and V. S. Popov, Phys. Rev. Lett. **104**, 220404 (2010).
[20] M. Jiang, W. Su, X. Lu, Z. M. Sheng, Y. T. Li, Y. J. Li, J. Zhang, R. Grobe, and Q. Su, Phys. Rev. A **83**, 053402 (2011).
[21] W. Su, M. Jiang, Z. Q. Lv, Y. J. Li, Z. M. Sheng, R. Grobe, and Q. Su, Phys. Rev. A **86**, 013422 (2012).
[22] Q. Su, W. Su, Z. Q. Lv, M. Jiang, X. Lu, Z. M. Sheng, and R. Grobe, Phys. Rev. Lett. **109**, 253202 (2012).
[23] F. Sauter, Z. Phys. **69**, 742 (1931).
[24] A. D. Bandrauk and H. Shen, J. Phys. A **27**, 7147 (1994).
[25] J. W. Braun, Q. Su, and R. Grobe, Phys. Rev. A **59**, 604 (1999).
[26] G. R. Mocken and C. H. Keitel, Comput. Phys. Commun. **178**, 868 (2008).
[27] M. Ruf, H. Bauke, and C. H. Keitel, J. Comput. Phys. **228**, 9092 (2009).
[28] P. Krekora, Q. Su, and R. Grobe, Phys. Rev. A **73**, 022114 (2006).
[29] A. I. Nikishov, Theor. Math. Phys. **20**, 653 (1974).
[30] S. P. Kim, H. K. Lee, and Y. Yoon, Phys. Rev. D **78**, 105013 (2008).
[31] S. P. Kim, H. K. Lee, and Y. Yoon, Phys. Rev. D **82**, 025015 (2010).
[32] M. Ruf, G. R. Mocken, C. Müller, K. Z. Hatsagortsyan, and C. H. Keitel, Phys. Rev. Lett. **102**, 080402 (2009).
[33] R. R. Freeman, P. H. Bucksbaum, H. Milchberg, S. Darack, D. Schumacher, and M. E. Geusic, Phys. Rev. Lett. **59**, 1092 (1987).
[34] R. E. Wagner, M. R. Ware, Q. Su, and R. Grobe, Phys. Rev. A **81**, 024101 (2010).
[35] R. E. Wagner, M. R. Ware, Q. Su, and R. Grobe, Phys. Rev. A **81**, 052104 (2010).